Tunable High-Q Plasmonic Metasurface with Multiple Surface Lattice Resonances

Nanxuan Wu[1, 2, 3], Yiyun Zhang[1, 2, 3], Hongbin Ma[1, 2, 3], Hongsheng Chen[1, 2, 3, *], and Haoliang Qian[1, 2, 3, *]

(*Invited*)

Abstract—Micro-nano opto-electronic devices are demanded to be highly efficient and capable of multiple working wavelengths in several light-matter interaction applications, which is a challenge to surface plasmonics owing to the relatively higher intrinsic loss and larger dispersion. To cross the barriers, a plasmonic metasurface combining both high Q-factors (highest $Q > 800$) and multiple resonant wavelengths is proposed by arranging step-staged pyramid units in lattice modes. Different numerical relations for nonlinear frequency conversions have been constructed because of its strong tunability. Also, characteristics of high radiation efficiency ($> 50\%$) and large localized optical density of state ($> 10^4$) have been proved through the numerical simulation. Such tunable high-Q metasurface can be implemented to quantum nonlinear process and enable the strong light-matter interaction devices into reality.

1. INTRODUCTION

Surface plasmonics, as the field mixed with photonics and electronics, have an astonishing progress with the development of the nano-technology in recent years [1]. The wavelengths of surface plasmonics are shorter than those of photons under the same frequency [2], which provides an effective strategy to break the diffraction limit and increase resolution. Plasmonic metasurfaces are artificially arranged with numbers of meta-atoms, resulting in specific electromagnetic characteristics and phenomena. Due to the subwavelength field confinement and easy-to-integrate characteristics, it is available to control light under miniaturization circumstances [3], such as chip-scale lenses [4] and spectrometers [5]. Moreover, higher radiation efficiency (RE) and larger localized optical density of state (LDOS) could be achieved with a dedicated design of plasmonic metasurfaces so that high-efficiency micro-nano opto-electronic devices can be realized. Generally, by changing the types of materials, structural sizes, nanoparticle shapes, and the periodic patterning, the effective mode index and the resonant frequency would change accordingly [6], therefore a customized reflectance and transmittance spectrum with the selected working points could be presented [7]. Concerning the powerful capabilities of light-field manipulation [8, 9], plasmonic metasurfaces can be used in light-matter interaction applications like biosensors [10], light-emitters [11], optical interconnector and modulators [12]. However, the intolerant high absorption under surface plasmonic resonances, introduced by the intrinsic electron-electron or electron-phonon interactions, causes significant losses and widens resonant bandwidths [13]. The loss leads to the challenge in some cutting-edge researches that continue to advance the interaction strength between

light and matter defined by Purcell factor [14], which is identified as the quality-factor (Q-factor) divided by the effective mode volume.

To break through the challenge, researchers have studied for years to reduce the effective mode volume to enhance the interaction strength [15, 16] while Q-factor has been commonly neglected in the plasmonic field, which describes the core radiative properties of the nanophotonic devices [17]. The high Q-factor resonances could reduce the losses, which is critical for the applications requiring ultra-sensitivity, ultra-resolution, and ultra-strong interaction, including the optical sensors, nonlinear wave-mixers [18], and quantum light sources [19]. Several types of high Q-factor modes have been studied to satisfy the frontier research requirements, including high-Q microcavities [20], plasmonic Fano resonances with suppressed radiative losses [21], and optical medium with gain [22]. However, these methods regularly cost relatively larger effective mode volumes or the enhancement of the Q-factor is limited within one order.

Recently, a new type of resonance, surface lattice resonance (SLR), has been proposed to overcome the low Q-factor limitation caused by the metallic loss, which increases the Q-factor by almost three orders [23, 24]. A strong coupling system has been achieved upon SLR, supporting Bose-Einstein condensation operating at room temperature [25]. Besides, due to the two-dimensional planar degrees of freedom, a doubly SLR metasurface consisting of arrays of L-shaped nanoparticles has been investigated on the enhancement of second-harmonic generation [26]. Unfortunately, the proposed high Q-factor metasurfaces only support one specific SLR with a certain polarization, which is still far away from the practical plasmonics-based devices requesting multiple working wavelengths, such as fluorescence imaging [27], display technologies [28], and frequency mixings [29]. To extend the functionality of SLR, a metasurface cladded by a dielectric layer is claimed to exhibit multiple hybrid SLR modes [30]. However, those multiple SLRs are hard to tune, and their multiple Q-factors are not high enough ($Q < 50$), indicating the dilemma of attaining both the high Q-factors and multiple tunable working points. In this paper, a metasurface composed of a rectangular array of step-staged pyramid (SSP) silver nanoparticles embedded in the silica environment is realized under a simple but exquisite design strategy, combining both multiple resonances and high Q-factors (MQ-metasurface). The designed metasurface supports at least three high-Q resonances (highest $Q > 800$), two orders of magnitude larger than that of the individual nanoparticles ($Q < 10$). A dipole simulation is carried out showing $30\% \sim 60\%$ radiation efficiency and three to four orders of magnitude enhancement for LDOS, which supports the large Purcell factor of MQ-metasurface for strong light-matter interactions. Furthermore, it is convenient to shift the multiple resonant wavelengths and build relations between them by tuning the geometrical parameters. Our proposed metasurface and design methodology would provide a solution to the miniaturization, tunability, and high efficiency of functional metasurfaces in nanophotonics and quantum optics, advancing further studies and applications such as single-photon sources and quantum entanglement sources.

In Figure 1(a), periodic arrangement of the SSP-nanoparticles cladded by dielectrics constitutes the MQ-metasurface, forming the lattice-type space, where designated SLR could exist. The geometrical parameters of the SSP-nanoparticles have been depicted in Figure 1(b), where each unit is composed of three layers of rectangular nanoparticles from the bottom to the top, shaping as a pyramid with step stages. The particle width w determines the wavelength of localized surface plasmonic resonance (LSPR), lattice periods P_x and P_y guarantee the SLR mode. Comparing with the single rectangular-shaped SLR unit, different particle lengths of each stage (L_1, L_2, and L_3) are the key parameters to tune the multiple working wavelengths. Figure 1(c) presents the electric-field distribution under the plane-wave excitation for one representative SSP unit featuring multiple resonances. The three-stage SSP units contain three P_y-determined SLR resonant modes (mode $h\nu1$, $h\nu2$, and $h\nu3$) and the electric-field confinements are different as responses of different stages. Each resonant mode can be tuned individually from corresponding geometrical parameters in different layers of the SSP unit. Combining the multiple high Q-factor resonances realized in MQ-metasurface, numerical relations between different resonant frequencies could be constructed, including $h\nu3 = h\nu2 + h\nu1$, $h\nu2 + h\nu2 - h\nu1 = h\nu3$, and $h\nu1 + h\nu4 - h\nu2 = h\nu3$ (with one additional high-Q resonant mode $h\nu4$ provided by one P_x-determined SLR resonant mode or hybridized between LSPR and Fano resonances), where the left parts of the equations represent the incident photons while the right parts are the generated ones.
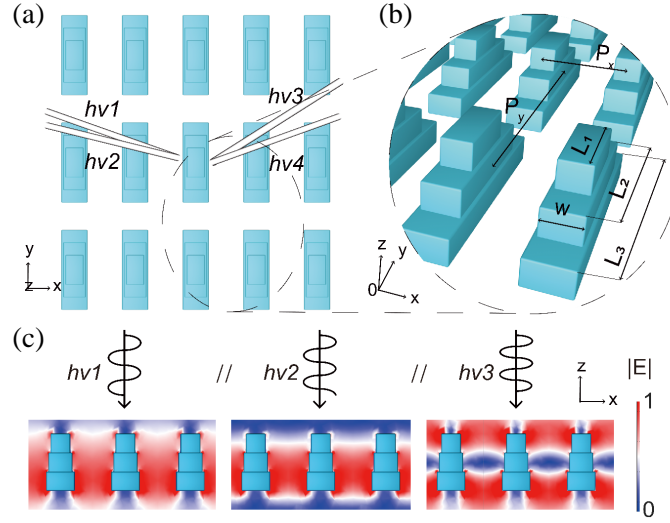
Figure 1. The proposed MQ-metasurface with geometrical structure design and its electric-field distributions. (a) MQ-metasurface consists of lattice arranged SSP units and possesses functions in wave-mixing between multiple photons with different wavelengths. The line indicates the absorbed or emitted photons, and the blue (white) part represents the silver SSP unit (silica). (b) Zoom-in schematics of the metasurface with the geometrical sizes and periods clearly marked. (c) The electric-field distributions of MQ-metasurface under the plane-wave excitation at three incident frequencies ($\nu1 < \nu2 < \nu3$). As the frequency becomes higher, the corresponding resonant electric-field distribution would be gradually confined to the narrower lattice space.

2. MODELING

Coupled Dipole Approximation or Lattice Sum Approach are helpful to the calculation modeling for SLR [23, 24, 31]. The relationship between the momentum $\vec{p}_i$ and the incident electric field $\vec{E}_{inc,i}$ of each nanoparticle in the periodic array can be obtained as $\vec{p}_i = \alpha^* \vec{E}_{inc,i}$ with the polarizability of dipoles under lattice distribution α^* defined as (See Supplementary Material Sec. 1 for full resonant condition analysis)

$$\alpha^* = \frac{\alpha_i}{1 - \alpha_i S} \vec{E}_{inc,i}. \tag{1}$$

The nanoparticle width w determines the LSPR polarizability α_i of a single particle. Here S is the lattice sum and is contributed by the lattice periods P_y and P_x. According to Eq. (1), α^* becomes maximum when $\text{Re}[1/\alpha_i - S] = 0$, which is the resonant condition of SLR. The lattice sum S helps to compensate for the loss caused by the metallic structures. The decreased imaginary part $\text{Im}[1/\alpha_i - S]$ could be decreased to near zero by choosing the appropriate periods, resulting in the increase of Q-factors. Along with the calculation approximation used in this research, the resonant wavelengths of MQ-metasurface are

$$\begin{aligned}
\lambda_{\text{SLR}\_i} &\approx n \cdot P, \quad i = 1, \\
\lambda_{\text{SLR}\_i} &\approx n \cdot (P - L_i/2), \quad i = 2, 3,
\end{aligned} \tag{2}$$

where n is the refractive index of the medium surrounding the nanoparticles, P the period, and L_i the particle length of the ith stage. When the particle sizes L_2 and L_3 are no longer far less than the lattice period, the rectangular unit can no longer be approximated as a dipole point and the resonant condition should be modified by considering the particle length as shown in Eq. (2). The Q-factors are calculated as $Q_i = \lambda_i/\Delta\lambda_i$, where $\Delta\lambda_i$ is the full width half maximum (FWHM) of the resonance.

As shown in the illustration from Figure 2(a), a simulation model of rectangular silver nanoparticles arranged in a rectangular array and embedded in silica has been constructed and studied (Method). The x-polarized incident light from the z-direction is applied to the metasurface with the nanoparticle width
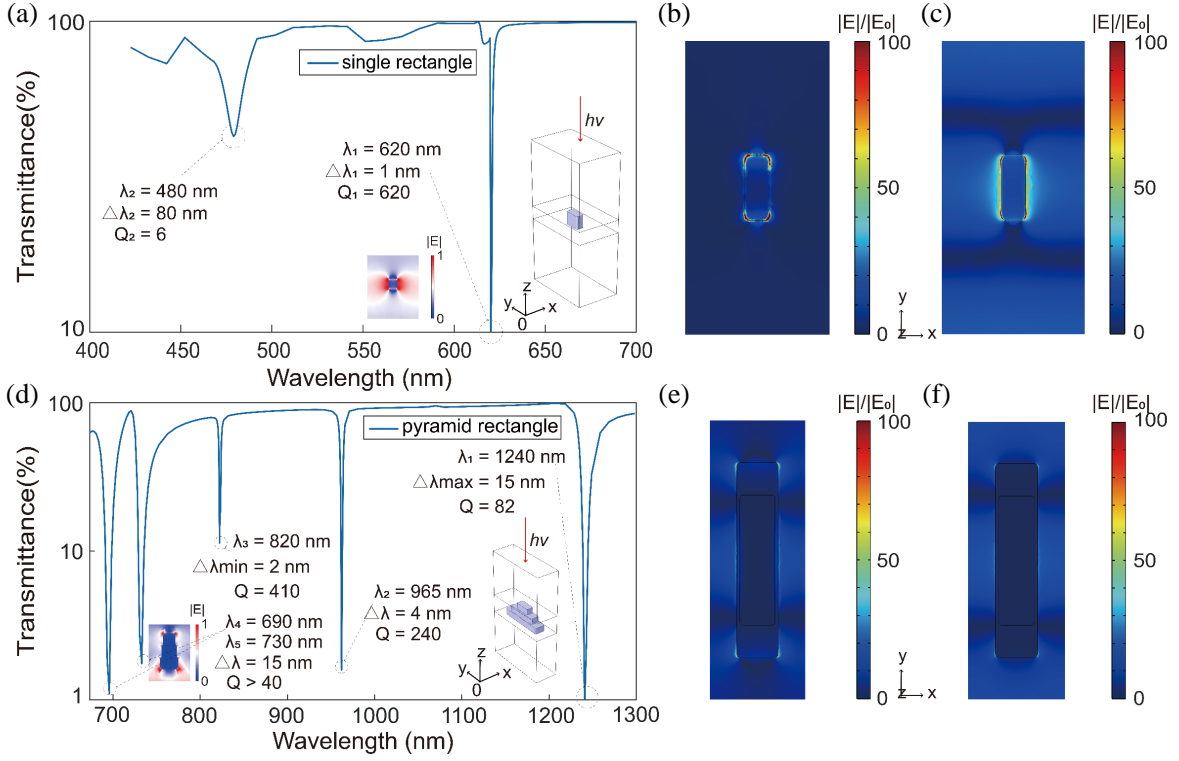
Figure 2. Simulation results for both single rectangular and SSP unit models. (a) Transmission spectrum for the rectangular unit model. The xz-plane electric-field distribution confirms the SLR resonant mode at $\lambda_1 = 620\,\text{nm} \approx n \cdot P = 1.46 \times 425\,\text{nm}$. (b), (c) The electric-field enhancements of single rectangular unit model with LSP and SLR resonant modes when the wavelengths of incident lights are (b) $\lambda_2 = 480\,\text{nm}$ and (c) $\lambda_1 = 620\,\text{nm}$. (d) Transmission spectrum of SSP unit for MQ-metasurface with the parameters set by $w = 110\,\text{nm}$, $P_x = 300\,\text{nm}$, $P_y = 860\,\text{nm}$, $L_1 = 200\,\text{nm}$, $L_2 = 400\,\text{nm}$, $L_3 = 600\,\text{nm}$. The wavelengths of five resonances are $\lambda_4 = 690\,\text{nm}$, $\lambda_5 = 730\,\text{nm}$, $\lambda_3 = 820\,\text{nm}$, $\lambda_2 = 965\,\text{nm}$, $\lambda_1 = 1240\,\text{nm}$. Three P_y-determined SLRs (λ_1, λ_2, λ_3) and one hybrid mode (λ_4) forms the equation $h\nu 1 + h\nu 4 - h\nu 2 = h\nu 3$. The largest Q-factor is 420 at the wavelength of $\lambda_3 = 820\,\text{nm}$. The xz-plane electric-field distribution shown in the inset is the mode analysis for hybrid modes. (e), (f) The mode analysis of SSP model at the highest-Q resonant wavelength of $\lambda_3 = 820\,\text{nm}$ and at the lowest-Q resonant wavelength of $\lambda_1 = 1240\,\text{nm}$. The electric-field enhancements in (e), (f) are calculated to demonstrate the interaction strength, where the maximum is among 80 and the average is 20-times.

$w = 45\,\text{nm}$, length $L_y = 95\,\text{nm}$, height $h = 100\,\text{nm}$, and the array periods $P_x = 260\,\text{nm}$, $P_y = 425\,\text{nm}$. This transmission spectrum contains both a wide bandwidth resonance (LSPR, $\Delta\lambda = 80\,\text{nm}$, $Q = 6$) and an extremely narrow bandwidth resonance (SLR, $\Delta\lambda = 1\,\text{nm}$, $Q = 620$) at two different wavelengths. The xy-plane electric-field enhancements in Figures 2(b)–(c) show that the LSPR mode (b) is mostly localized at the interface of metal and dielectric while it covers the whole lattice space under the SLR mode (c).

The single rectangular-shaped SLR unit metasurface has one high-Q resonance which can be easily tuned by changing the period. Hence, a solution to multiple SLRs is realized by combining multiple single rectangular units together as one SSP unit (Method). The simulation result shown in Figure 2(d) proves the prediction that three rectangular nanoparticles would support three P_y-determined SLR modes. Besides, the three resonant wavelengths can be independently tuned by changing the period P_y and the particle length L_i of each stage in the y-direction. Three P_y-determined SLR modes all follow the theoretical analysis Eq. (2) ($\lambda_1 = 1240\,\text{nm} \approx n \cdot P_y = 1.46 \times 860\,\text{nm}$, $\lambda_2 = 965\,\text{nm} \approx n \cdot (P_y - L_2/2) = 1.46 \times 660\,\text{nm}$, $\lambda_3 = 820\,\text{nm} \approx n \cdot (P_y - L_3/2) = 1.46 \times 560\,\text{nm}$). The

electric-field enhancements for the highest-Q ($\Delta\lambda_{\min} = 2\,\text{nm}$, $Q = 410$) and lowest-Q ($\Delta\lambda_{\min} = 15\,\text{nm}$, $Q = 80$) SLR modes shown in Figures 2(e)–(f) are similar to Figure 2(c), which demonstrates that the multiple resonant modes are all SLRs or SLR-dominated hybrid-resonant modes. Furthermore, the surrounding silica is designed as a thick cladding layer ($t = 720\,\text{nm}$) to hybridize the LSPR resonant mode and the Fano resonance effect between the SSP metallic structure and the dielectric-air interface mentioned in Ref. [30], resulting in hybrid SLR modes ($\lambda_4 = 690\,\text{nm}$, $\lambda_5 = 730\,\text{nm}$) shown in the inset in Figure 2(d) with enhanced Q-factors. To construct a clear and simplified transmission spectrum, the three LSPR peaks for the SSP unit are degenerated by setting similar width w of each nanoparticle. Meanwhile, the lattice spaces in x-direction for three layers are also similar, resulting in the degenerated P_x-determined SLRs. Thus, apart from three P_y-determined SLRs, only one hybrid mode ($\lambda_{\text{hybrid}} \approx \lambda_{\text{LSPR}}$) and one P_x-determined SLR ($\lambda_{P_x} \approx n \cdot P_x$) exists. However, the step size in x-direction Δw of SSP unit is still critical to the electric-field enhancement as it would greatly affect the effective mode volume and the Purcell factor [32] (see Supplementary Material Sec. 2 for the design stratagem of the step size in x-direction).
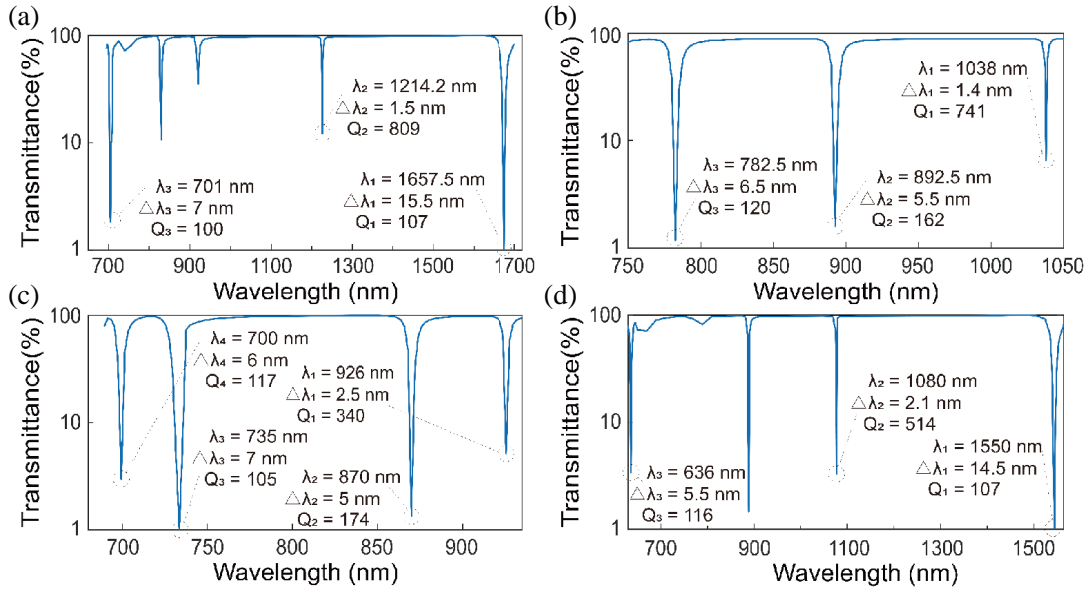

Figure 3. Spectrum of four MQ-metasurfaces for different applications. To avoid high-order hybrid modes influencing the selected working wavelengths, the thicknesses of silica cladding on the SSP units of four MQ-metasurfaces are only 200 nm. (a) Transmission spectrum for quantum parameter down-conversion with the parameters set by $w = 110\,\text{nm}$, $P_x = 500\,\text{nm}$, $P_y = 1990\,\text{nm}$, $L_3 = 285\,\text{nm}$, $L_2 = 685\,\text{nm}$, $L_1 = 1085\,\text{nm}$. Here two P_y-determined SLRs ($\lambda_2 = 1214.2\,\text{nm}$, $\lambda_1 = 1657.5\,\text{nm}$) and one hybrid mode ($\lambda_3 = 701\,\text{nm}$) can form the equation $\frac{hc}{\lambda_3} = \frac{hc}{\lambda_2} + \frac{hc}{\lambda_1}$. (b) Transmission spectrum for degenerated FWM with the parameters set by $w = 110\,\text{nm}$, $P_x = 505\,\text{nm}$, $P_y = 1600\,\text{nm}$, $L_1 = 368\,\text{nm}$, $L_2 = 560\,\text{nm}$, $L_3 = 752\,\text{nm}$. Here P_y-determined SLRs ($\lambda_3 = 782.5\,\text{nm}$, $\lambda_2 = 892.5\,\text{nm}$, $\lambda_1 = 1038\,\text{nm}$) can form the equation $\frac{hc}{\lambda_2} + \frac{hc}{\lambda_2} - \frac{hc}{\lambda_1} = \frac{hc}{\lambda_3}$. (c) Transmission spectrum for FWM involving single photon source with the parameters set by $w = 110\,\text{nm}$, $P_x = 505\,\text{nm}$, $P_y = 1360\,\text{nm}$, $L_1 = 240\,\text{nm}$, $L_2 = 440\,\text{nm}$, $L_3 = 640\,\text{nm}$. Here two P_y determined SLRs ($\lambda_2 = 870\,\text{nm}$, $\lambda_1 = 926\,\text{nm}$), one hybrid mode ($\lambda_4 = 700\,\text{nm}$), and one P_x determined SLR ($\lambda_3 = 735\,\text{nm}$) can form the equation $\frac{hc}{\lambda_1} + \frac{hc}{\lambda_4} - \frac{hc}{\lambda_2} = \frac{hc}{\lambda_3}$. (d) Transmission spectrum for frequency conversion of specific optical communication wavelengths with the parameters set by $w = 110\,\text{nm}$, $P_x = 429\,\text{nm}$, $P_y = 1680\,\text{nm}$, $L_1 = 422\,\text{nm}$, $L_2 = 662\,\text{nm}$, $L_3 = 902\,\text{nm}$. Here two P_y-determined SLRs ($\lambda_2 = 1080\,\text{nm}$, $\lambda_1 = 1550\,\text{nm}$) and one P_x-determined SLR ($\lambda_3 = 636\,\text{nm}$) can form the equation $\frac{hc}{\lambda_3} = \frac{hc}{\lambda_2} + \frac{hc}{\lambda_1}$.

3. RESULTS

The regular rectangular shape provides the MQ-metasurface with advantages that the resonant wavelengths are easy to be analyzed and tuned by changing the periods and size parameters. For example, when the largest resonant wavelength is determined by P_y, it is convenient to tune the other two P_y-determined SLR wavelengths of the metasurface by changing the size parameters L_i of each stage. Forming numerical equations with the multiple resonant wavelengths can be implemented as nonlinear frequency conversions, such as the four wave-mixing (FWM) $h\nu1 + h\nu4 - h\nu2 = h\nu3$ realized by four resonances in Figure 2(d) including 690 nm, 820 nm, 965 nm, and 1240 nm.

Here in Figure 3, transmission spectra of four representative MQ-metasurfaces have been presented to construct specific functions. All the resonant modes (three P_y-determined SLRs, one P_x-determined SLR, and one hybrid mode) are chosen from their best tuning range to construct the equations (see Supplementary Material Sec. 1, Sec. 3). Using three of the high-Q resonances shown in Figure 3(a), equation $h\nu3 = h\nu2 + h\nu1$ can be constructed to prepare an entangled quantum photon source through parametric down-conversion [33]. In addition, because of the multiple degrees of freedom, for the same case with three resonant wavelengths, the wavelengths can be tuned to form a degenerated FWM as $h\nu2 + h\nu2 - h\nu1 = h\nu3$, which can be used to realize entangled photon-pair generation [34] with the data shown in Figure 3(b). Besides, combining the four high Q-factor resonances shown in Figure 3(c), the single photon involved FWM can be realized through the equation $h\nu1 + h\nu4 - h\nu2 = h\nu3$ [35]. Moreover,
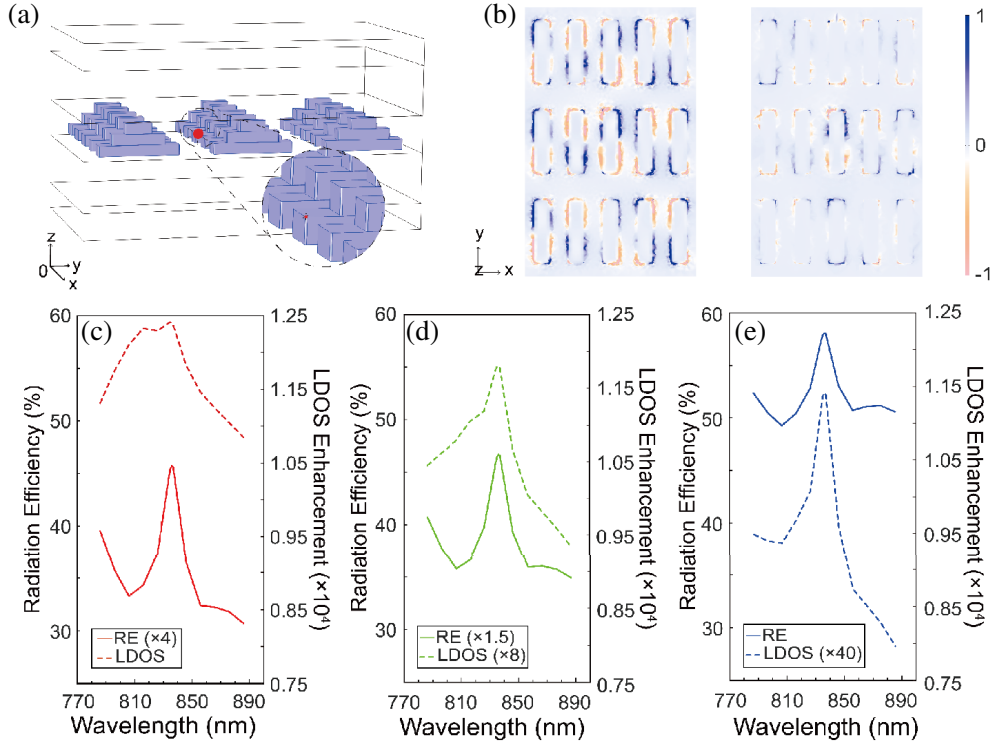

Figure 4. Results for LDOS and RE using the dipole simulation. (a) Scheme of the dipole simulation where the red point situated at the corner of the SSP unit is the dipole. The geometrical parameters are the same as the simulation mentioned in Figure 2(d). (b) Charge distributions of the system under the resonant wavelength ($\lambda = 836$ nm, left) and the wavelength without resonance ($\lambda = 886$ nm, right). Under the normalized color bar, the left charge distribution is uniformly distributed in the whole lattice space, while the right one is mostly localized at the corners of the particles. (c)–(e) RE (solid line) and LDOS enhancement (dashed line)for the designed resonant wavelength. The distances between the dipole and nearest SSP unit varies from 0.2 nm (red) to 1 nm (green) and 2 nm (blue). Noted that both the highest RE and LDOS are obtained under the same wavelength ($\lambda = 836$ nm) for three distances.

MQ-metasurfaces working at optical communication wavelengths ($\lambda_2 = 1080$ nm, $\lambda_1 = 1550$ nm) have been proposed with the spectrum (same numerical relation as Figure 3(a)) shown in Figure 3(d), proving the intense tunable capability. Due to the high-Q resonant features, the accuracy of the numerical relations based on the designed multiple SLR wavelengths needs to be carefully considered. We set the design principle to guarantee the accuracy of the numerical relations where the deviation of the numerical relations should be less than the FWHM of the resonances in the frequency domain Δv, taking the first equation shown in Figure 3(a) as an example $|hv_3 - (hv_2 + hv_1)| < |h\Delta v|_{\min}$. It is worth noting that all the relations listed above satisfy the requirement well, and the tuning optimization details have been given in Supplementary Material Sec. 3.

The designed frequency conversions based on multiple resonances with high Q-factors are aimed at the applications of the strong light-matter interactions, and the two characteristics of the MQ-metasurface including the high Q-factor and multi-wavelength resonances are the bases for quantum nonlinear processes. The highest electric-field enhancement of the MQ-metasurface shown in Figure 3(d) is up to 250 times, which indicates the strong interaction strength and advances the potentials of MQ-metasurface based applications (see Supplementary Material Sec. 4). To prove the feasibility, the LDOS and RE of MQ-metasurface are studied by the dipole simulation shown in Figure 4(a), representing the interaction strength between the dipole and SSP units. The charge distribution comparison in Figure 4(b) guarantees the SLR mode. In Figures 4(c)–(e), different figures are obtained by placing the dipole at the corner of the SSP unit with different distances. The highest enhancement of the RE at the resonance is above 50%, and the highest enhancement of LDOS is above 12000, which reflects the low-loss resonant mode, proves the strong interaction strength [36], and promotes the realization of the quantum nonlinear process.

4. DISCUSSIONS

Though expanding the high Q-factor resonant mode (SLR) to multiple working wavelengths is the main research objective, other methods to enhance the Q-factor can be combined in this MQ-metasurface design as well. The silica in the lattice space could be replaced by the optical medium with gain to further compensate for the loss. Besides, organizing arrays with hyper-periodicities consisting of finite arrays of SSP units (superlattice mode) may provide even narrower linewidth. If more resonant modes are demanded, staking additional nanoparticles would be acceptable. In terms of the fabrication, MQ-metasurface can be well integrated with the micro-nano processing, including the lithography and film deposition which are compatible with the standard CMOS technology [24, 37, 38]. It is worth noting that the acceptable misalignment during the multiple lithography process has been discussed in Supplementary Material Sec. 5. Moreover, the low-loss feature of the SLR mode is especially significant to the quantum information manipulation, as a solution for implementing quantum algorithms and building quantum information processors [39].

5. CONCLUSIONS

In summary, multiple high-Q resonances have been achieved by MQ-metasurface composed of SSP units under a simple but exquisite design strategy. Due to the low-loss SLR modes, the high Q-factors (highest $Q > 800$) are guaranteed by arranging the SSP units in rectangular arrays and confining the electric field in the lattice space. SSP units provide additional degrees of freedom than single rectangular shaped units, which results in the strong tunability to tune each working wavelength individually. Thus, MQ-metasurface with customized numerical relations between multiple resonances could be straightforwardly implemented as different quantum frequency conversion metasurfaces. Besides, the rationality that MQ-metasurface can be used in the applications of strong light-matter interactions has been proved through the dipole simulations. Combining other photonic/plasmonic nanostructures and quantum physics, our proposed MQ-metasurface and design methodology may make novel quantum-optical devices with miniaturization, tunability, and high efficiency one more step into reality.

6. METHOD

Numerical Simulation

Numerical finite-element simulations including the optical transmittance, the cross-section mode analysis, the radiative and non-radiative power calculations were performed with the COMSOL Multiphysics.

Author Contributions

H. Q. and N. W. conceived the idea. N. W. conducted the numerical simulations. N. W. and H. Q. contributed extensively to the writing of the manuscript. N. W., Y. Z., H. M., H. C., and H. Q. analyzed data and interpreted the details of the results. H. C. and H. Q. supervised the research.

Declaration of Competing Interest

The authors declare no competing interests.

Data Availability Statement

The data that supports the plots within this letter and other findings of this study are available from the corresponding author upon reasonable request.

REFERENCES

1. Fernández-Domínguez, A., F. Garcia-Vidal, and L. Martín-Moreno, "Unrelenting plasmons," *Nat. Photonics*, Vol. 11, 8–10, 2017.
2. De Bruijn, H. E., R. P. H. Kooyman, and J. Greve, "Choice of metal and wavelength for surface-plasmon resonance sensors: Some considerations," *Appl. Opt.*, Vol. 31, 440–442, 1992.
3. Arbabi, A., et al., "Miniature optical planar camera based on a wide-angle metasurface doublet corrected for monochromatic aberrations," *Nat. Commun.*, Vol. 7, 13682, 2016.
4. Li, L., et al., "Metalens-array-based high-dimensional and multiphoton quantum source," *Science*, Vol. 368, 1487–1490, 2020.
5. Yu, N. and F. Capasso, "Flat optics with designer metasurfaces," *Nat. Mater.*, Vol. 13, 139–150, 2014.
6. Kelly, K. L., E. Coronado, L. L. Zhao, and G. C. Schatz, "The optical properties of metal nanoparticles: The influence of size, shape, and dielectric environment," *J. Phys. Chem. B*, Vol. 107, 668–677, 2003.
7. Liu, H. and P. Lalanne, "Microscopic theory of the extraordinary optical transmission," *Nature*, Vol. 452, 728–731, 2008.
8. Zhao, Y. and A. Alù, "Manipulating light polarization with ultrathin plasmonic metasurfaces," *Phys. Rev. B*, Vol. 84, 205428, 2011.
9. Karimi, E., et al., "Generating optical orbital angular momentum at visible wavelengths using a plasmonic metasurface," *Light Sci. Appl.*, Vol. 3, e167, 2014.
10. Alipour, A., A. Farmani, and A. Mir, "High sensitivity and tunable nanoscale sensor based on plasmon-induced transparency in plasmonic metasurface," *IEEE Sens. J.*, Vol. 18, 7047–7054, 2018.

11. Vaskin, A., R. Kolkowski, A. F. Koenderink, and I. Staude, "Light-emitting metasurfaces," *Nanophotonics*, Vol. 8, 1151–1198, 2019.

12. Kamali, S. M., E. Arbabi, A. Arbabi, and A. Faraon, "A review of dielectric optical metasurfaces for wavefront control," *Nanophotonics*, Vol. 7, 1041–1068, 2018.

13. Emani, N. K., et al., "High-efficiency and low-loss gallium nitride dielectric metasurfaces for nanophotonics at visible wavelengths," *Appl. Phys. Lett.*, Vol. 111, 221101, 2017.

14. Purcell, E. M., *Confined Electrons and Photons: New Physics and Applications*, E. Burstein and C. Weisbuch, 839, Springer US, Boston, MA, 1995.

15. Schuller, J. A., et al., "Plasmonics for extreme light concentration and manipulation," *Nat. Mater.*, Vol. 9, 193–204, 2010.

16. Agio, M. and D. M. Cano, "The Purcell factor of nanoresonators," *Nat. Photonics*, Vol. 7, 674–675, 2013.

17. Boriskina, S. V., T. A. Cooper, L. Zeng, G. W. Ni, and C. Gang, "Losses in plasmonics: From mitigating energy dissipation to embracing loss-enabled functionalities," *Adv. Opt. Photonics*, Vol. 9, 775–827, 2017.

18. Aouani, H., et al., "Multiresonant broadband optical antennas as efficient tunable nanosources of second harmonic light," *Nano Lett.*, Vol. 12, 4997–5002, 2012.

19. Walmsley, I. A., "Quantum optics: Science and technology in a new light," *Science*, Vol. 348, 525–530, 2015.

20. Zhang, Q., S. T. Ha, X. Liu, T. C. Sum, and Q. Xiong, "Room-temperature near-infrared high-Q perovskite whispering-gallery planar nanolasers," *Nano Lett.*, Vol. 14, 5995–6001, 2014.

21. Chen, J., F. Gan, Y. Wang, and G. Li, "Plasmonic sensing and modulation based on fano resonances," *Adv. Opt. Photonics*, Vol. 6, 1701152, 2018.

22. Ma, R., R. F. Oulton, V. J. Sorger, G. Bartal, and X. Zhang, "Room-temperature sub-diffraction-limited plasmon laser by total internal reflection," *Nat. Mater.*, Vol. 10, 110–113, 2011.

23. Kravets, V. G., A. V. Kabashin, W. L. Barnes, and A. N. Grigorenko, "Plasmonic surface lattice resonances: A review of properties and applications," *Chem. Rev.*, Vol. 118, 5912–5951, 2018.

24. Bin-Alam, M. S., et al., "Ultra-high-Q resonances in plasmonic metasurfaces," *Nat. Commun.*, Vol. 12, 974, 2021.

25. Hakala, T. K., et al., "Bose-Einstein condensation in a plasmonic lattice," *Nat. Phys.*, Vol. 14, 739–744, 2018.

26. Huttunen, M., et al., "Efficient nonlinear metasurfaces by using multiresonant high-Q plasmonic arrays," *J. Opt. Soc. Am. B*, Vol. 36, E30, 2019.

27. Kinkhabwala, A., et al., "Large single-molecule fluorescence enhancements produced by a bowtie nanoantenna," *Nat. Photonics*, Vol. 3, 654–657, 2009.

28. Hsu, C. W., et al., "Transparent displays enabled by resonant nanoparticle scattering," *Nat. Commun.*, Vol. 5, 3152, 2014.

29. Krasnok, A., M. Tymchenko, and A. Alù, "Nonlinear metasurfaces: A paradigm shift in nonlinear optics," *Mater.*, Vol. 21, 8–21, 2018.

30. Reshef, O., et al., "Multiresonant high-Q plasmonic metasurfaces," *Nano Lett.*, Vol. 19, 6429–6434, 2019.

31. Purcell, E. and C. Pennypacker, "Scattering and absorption of light by nonspherical dielectric grains," *Astrophys. J.*, Vol. 186, 705–714, 1973.

32. Sauvan, C., J. Hugonin, I. Maksymov, and P. Lalanne, "Theory of the spontaneous optical emission of nanosize photonic and plasmon resonators," *Phys. Rev. Lett.*, Vol. 110, 2013.

33. Kwiat, P. G., E. Waks, A. G. White, I. Appelbaum, and P. H. Eberhard, "Ultrabright source of polarization-entangled photons," *Phys. Rev. A*, Vol. 60, R773, 1999.

34. Reimer, C., et al., "Cross-polarized photon-pair generation and bi-chromatically pumped optical parametric oscillation on a chip," *Nat. Commun.*, Vol. 6, 8236, 2015.

35. Saffman, M. and T. G. Walker, "Creating single-atom and single-photon sources from entangled atomic ensembles," *Phys. Rev. A*, Vol. 66, 065403, 2002.

36. Lu, D., J. Kan, E. Fullerton, and Z. Liu, "Enhancing spontaneous emission rates of molecules using nanopatterned multilayer hyperbolic metamaterials," *Nat. Nanotechnol.*, Vol. 9, 48–53, 2014.

37. Vieu, C., et al., "Electron beam lithography: Resolution limits and applications," *Appl. Surf. Sci.*, Vol. 164, 111–117, 2000.

38. Wang, K., H. Qian, Z. Liu, and P. K. L. Yu, "Second-order nonlinear susceptibility enhancement in gallium nitride nanowires (invited)," *Progress In Electromagnetics Research*, Vol. 168, 25–30, 2020.

39. Zhong, H.-S., et al., "Quantum computational advantage using photons," *Science*, Vol. 370, 1460–1463, 2020.